

Spatial drought reconstructions for central High Asia based on tree rings

Keyan Fang · Nicole Davi · Xiaohua Gou ·
Fahu Chen · Edward Cook · Jinbao Li ·
Rosanne D'Arrigo

Received: 15 February 2009 / Accepted: 28 December 2009 / Published online: 7 January 2010
© Springer-Verlag 2010

Abstract Spatial reconstructions of drought for central High Asia based on a tree-ring network are presented. Drought patterns for central High Asia are classified into western and eastern modes of variability. Tree-ring based reconstructions of the Palmer drought severity index (PDSI) are presented for both the western central High Asia drought mode (1587–2005), and for the eastern central High Asia mode (1660–2005). Both reconstructions, generated using a principal component regression method, show an increased variability in recent decades. The wettest epoch for both reconstructions occurred from the 1940s to the 1950s. The most extreme reconstructed drought for western central High Asia was from the 1640s to the 1650s, coinciding with the collapse of the Chinese Ming Dynasty. The eastern central High Asia reconstruction has shown a distinct tendency towards drier conditions since the 1980s. Our spatial reconstructions agree well with previous reconstructions that fall within each mode, while there is no significant correlation between the two spatial reconstructions.

Keywords Tree-ring · PDSI · Central High Asia · Principal component regression

K. Fang · X. Gou (✉) · F. Chen
Key Laboratory of Western Chinese Environmental Systems
(MOE), Center for Arid Environment and Paleoclimate Research
(CAEP), Lanzhou University, 730000 Lanzhou, China
e-mail: xhgou@lzu.edu.cn

K. Fang
e-mail: kujanfang@gmail.com

K. Fang · N. Davi · E. Cook · J. Li · R. D'Arrigo
Tree-Ring Lab, Lamont-Doherty Earth Observatory,
Columbia University, Palisades, NY 10964, USA

1 Introduction

Shifts in moisture patterns over central High Asia in recent decades are a serious concern due to their significant impacts on regional water resources management for this arid area (Shi et al. 2007). One limitation on our understanding of drought regimes in this area is the short instrumental records. Most records only became available in the 1950s. This situation can be mitigated via a paleoclimatic perspective, employing an annually resolved, exactly dated proxy records such as tree-rings (Fritts 1991). Tree-ring based drought reconstructions available in this area are focused on specific sites or a small region (e.g. Davi et al. 2006, 2009; Fang et al. 2009a, b; Li et al. 2006, 2007; Liu et al. 2004; Tian et al. 2007; Yuan et al. 2003). Climate reconstruction for a geographic point in a heterogeneous area provides a less comprehensive picture of regional drought when compared to spatial field reconstructions (Briffa et al. 1986; Cook et al. 1994, 2002, 2004; D'Arrigo and Wilson 2006; Fritts 1991; Meko et al. 1993). Furthermore, spatial reconstructions have the advantage of being readily comparable to modeling results that test the underlying forcing mechanisms (Cook et al. 1994).

Spatial drought reconstructions with the use of a tree-ring network have been developed for many areas, such as Europe, North America and Mongolia (e.g. Briffa et al. 1986; Cook et al. 1994, 1999, 2004; Davi et al. 2010; Haston and Michaelsen 1997; Meko et al. 1993). Herein, we present a spatial reconstruction with a focus on central High Asia (70E–112E, 33N–52N) based on a 130-chronology tree-ring network. Previous studies using instrumental data indicated that the moisture conditions in central High Asia are highly variable (Li et al. 2009; Qian and Qin 2008; Zou et al. 2005). For example, the eastern portion of this region showed a persistent drying trend,

while a wetting trend was observed since the 1980s for the western part (Shi et al. 2007; Davi et al. 2009). Due to the heterogeneity of moisture patterns in this sizable area, we first classify the moisture patterns based on the available instrumental records and then reconstruct the distinguished drought fields. The goals of this study are to: (1) identify the leading drought patterns for central High Asia, (2) use the tree-ring network to reconstruct each identified drought mode; and (3) investigate the variability of each reconstruction and explore the relationships between them. We briefly describe the tree-ring network, climate data and the analytical techniques in Sect. 2. In Sect. 3, the drought patterns are classified based on instrumental PDSI data, the identified spatial drought modes are reconstructed, and the reconstructions are compared using running cross-correlations. Discussion and conclusions are presented in Sects. 4 and 5, respectively.

2 Data and methods

2.1 Tree-ring network

The study region, located in central High Asia, is characterized by a cold and dry climate. The driest areas are found in lowlands where annual precipitation can drop below 50 mm, such as the Tarim and Dzungarian basins. Relatively higher precipitations are seen in high mountain ranges, such as the northern Tibetan Plateau and Tianshan Mountains. Most tree-ring sites are collected from high-elevation sites (higher than about 2000 m a.s.l.) in the mountain ranges where old-growth forests could be found. Our tree-ring network is composed of 130 ring-width and a few density chronologies across central High Asia that share a common period from 1774 to 1990 (Table 1). Site locations of these candidate tree-ring chronologies are shown in Fig. 1, where some circles represent more than one chronology. The uneven distribution of sampling sites is caused by the patchiness of natural forest cover in this area. All the chronologies are derived from coniferous tree species (Pinaceae and Cupressaceae), including *Larix sibirica* (71 chronologies), *Pinus sibirica* (4), *Pinus sylvestris*

(1), *Pinus flexilis* (1), *Pinus aristata* (1), *Pinus tabuliformis* (1), *Tsuga chinensis* (1), *Picea schrenkiana* (14), *Juniperus przewalskii* (24), and *Juniperus turkestanica* (12). The averaged growth rate (AGR, mm/year) is calculated as the ratio between all ring-widths and the total number of tree rings within each site, which is compared to the mean segment length (MSL). Averaged absolute correlations of tree-growth to PDSI in previous and current years are compared to the elevation of each site, in order to explore the relations of drought sensitivity to elevations.

A large portion of these chronologies have been used in previous climate reconstructions for geographic points or small regions (e.g. Davi et al. 2006, 2009; D'Arrigo et al. 2000; Fang et al. 2009a, b; Li et al. 2006, 2007; Tian et al. 2007). In order to preserve as much low-frequency signal as possible, we detrended most of the raw tree-ring measurements using straight lines or negative exponential curves. Tree-ring series with significant non-climatic disturbances that cannot be fitted well by conservative curves were detrended by a rigid cubic spline curve with a 50% cutoff equal to 2/3 of each series' length. Although there is uncertainty about the frequency properties recovered from

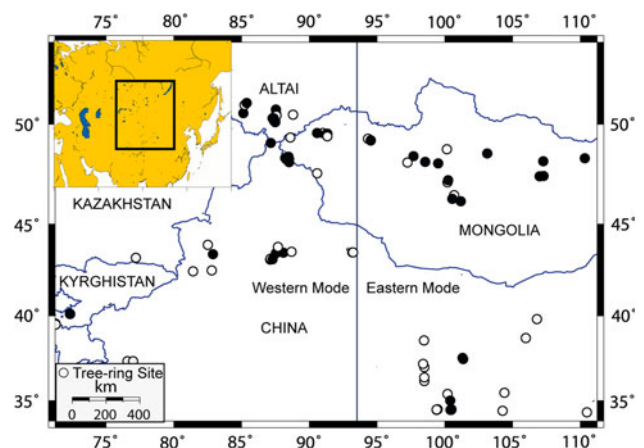


Fig. 1 Location map of tree-ring sites used in this study. Some locations represent more than one chronology. The line at 93.75E indicates the delimitation between the western and eastern drought modes, as will shown in Fig. 4. The filled circles show significant (0.10 level) correlations with regional droughts

Table 1 Information on the regional tree-ring chronologies before and after reconstruction

Region	Number of chronologies	Full coverage	Mean chronology length	Reliable ^a mean length	Number of retained chronologies	Number of retained predictors	Number of PDSI grids
Entire region	130	0–2005	551	470			
Western ^b mode	81	694–2005	642	385	38	48	90
Eastern ^b mode	49	0–2004	672	555	19	25	63

^a Reliable periods of chronologies are based on the number of the radii greater than 6

^b The western and eastern modes are based on classification as shown in Fig. 3

tree rings, we believe that at least the centennial-scale climate variability could be reconstructed using the conservative detrending methods and centuries long segment lengths of chronologies (Table 1). Detrended tree-ring series were averaged to generate tree-ring chronologies based on a robust mean methodology (Cook 1985). In order to better retain low-frequency variation, we mainly utilized the standard (104 chronologies) and ARSTAN (26) chronologies (Cook 1985). Prior to regression analyses, tree-ring chronologies were assessed for signal strength and only those time intervals with more than six measurable individual series were utilized. This criterion determines the portions for which the chronologies are relatively reliable (Meko et al. 1993; Cook et al. 1999).

2.2 PDSI data

We utilize the Palmer drought severity index (PDSI), a measure of accumulated moisture deficit relative to local mean moisture conditions (Palmer 1965; Dai et al. 2004). PDSI is probably the most commonly used drought index for tree-ring based reconstructions across the globe (e.g. Meko et al. 1993; Cook et al. 1999; 2004), including central High Asia (e.g. Davi et al. 2009; Fang et al. 2009a, b; Li et al. 2006, 2007; Tian et al. 2007). The global PDSI network employed herein was developed by Dai et al. (2004), which features a $2.5^\circ \times 2.5^\circ$ gridding system covering the period of 1951–2005, the common period for most grids in this region (Li et al. 2009). Since the PDSI model is more accurate for warm season soil moisture contents (Dai et al. 2004), we calibrated tree-ring chronologies in previous and current years using the warm season PDSI from May to September.

2.3 Methods

Rotated principal component analysis (RPCA), using the varimax method (Richman 1986), was employed to identify spatial drought patterns over central High Asia based on instrumental PDSI data from 1951 to 2005. In order to reconstruct the leading drought modes for central High Asia, we utilized the principal component regression method (Briffa et al. 1986; Cook et al. 2002). Prior to regression, the candidate tree-ring chronologies were screened using correlation analyses with a cutoff probability at the 0.10 significance level. The retained moisture sensitive tree-ring chronologies and the PDSI network were both decomposed by PCA to generate reduced sets of orthogonal eigenvectors. We removed the higher-order tree-ring eigenvectors that accounted for little variance, i.e. those with eigenvalues lower than 1, which is able to reduce the level of artificial predictability caused by the inclusion of spurious predictors (Cook et al. 1994). In this

study, only the first principal component (PC) of the PDSI field was retained in regression analysis, in order to reconstruct the leading pattern of each drought mode. With regards to the remaining tree-ring PC eigenvectors, the minimum AIC criterion was employed to determine the predictors for the final regression model.

In order to generate the longest possible reconstructions, a series of nested regression models were developed by stepwise shifting backward the common starting year in 15-year increments (Cook et al. 2002; D'Arrigo and Wilson 2006). For each nested regression model, a split calibration–verification procedure was used to test the model reliability (Meko and Graybill 1995). That is, the full period was divided into two sub-periods, with the calibration model developed from one sub-period verified against the remaining data from the other. Since the common period between tree rings and PDSI is very short (1951–1992), we used a relatively longer 30-year calibration period to guarantee the calibration model stability in the split calibration and verification procedure. A number of statistics were employed to evaluate the model ability, i.e. r square, reduction of error (RE), and coefficient of efficiency (CE). Values of RE and CE greater than zero indicate acceptable model skill (Cook et al. 1999). The length of the final reconstruction equals the longest nested regression model that still has good calibration and verification results. All nested reconstructions were rescaled to the most replicated common period to produce a final reconstruction with theoretically stable variance between the time-varying nested reconstructions (Cook et al. 2002).

The west and east mode reconstructions were compared with a far-western Mongolia PDSI reconstruction (Davi et al. 2009) and Selenge streamflow reconstruction in Mongolia (Davi et al. 2006), respectively, which were focused on small areas in our study region. The west and east mode reconstructions were compared to investigate their inter-relationships. Running correlations were calculated in order to quantitatively evaluate the time-varying relationships, using a 51-year running window. Spectral properties of both reconstructions were investigated using a multi-taper method (MTM), a powerful tool in spectral estimation that is particularly effective for short time series (Mann and Lee 1996).

3 Results

As shown in Fig. 2a, a clear decline trend of AGR is seen along with the increase in MSL. Opposing variability is also seen between the drought responses and elevations, although the trend is not strong (Fig. 2b). The first two PCs of the instrumental PDSI explain 35.8% of the total variance over the study region (Table 2). The rotated first PC

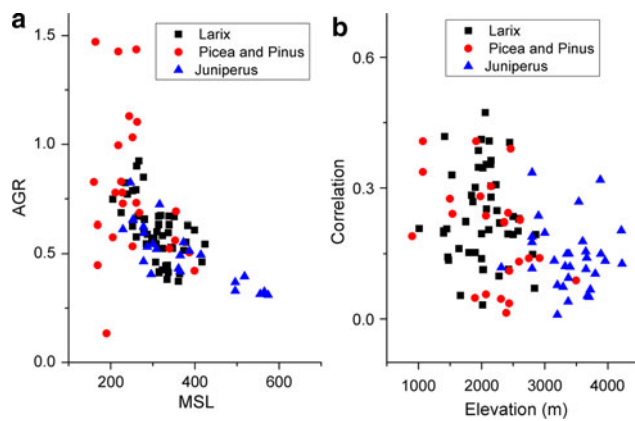


Fig. 2 Comparisons between (a) mean segment length (MSL) and averaged growth rate (AGR), as well as (b) between elevation (meter above sea level) and correlation of tree-growth to averaged drought responses of the previous and current years. All the tree species are classified into three types: *Juniperus* (triangle), *Larix* (square), *Pinus* and *Picea* (circle)

of the instrumental data is most heavily loaded over western central High Asia, i.e. Kazakhstan, westernmost China, western Mongolia, and Kyrgyzstan (Fig. 3). Therefore we call the first rotated PC the “western mode”. The second rotated PC, yielding the highest loadings over the eastern study region (Fig. 3), is referred to as the “eastern mode”. The western and eastern modes are arbitrarily divided by the loading coefficient of 0.4, near 93.75E (Figs. 3, 4). The first PCs of the western and eastern drought modes are retained for the following regression analysis (Fig. 4; Table 2). The first principal components of the western and eastern drought modes explain 32.5 and 33.7% of the total variance, respectively. Low loadings are seen on the Tibetan Plateau that is southern to the study region (Fig. 4; Table 2). Eighty-one (49) chronologies falling within the western (eastern) domain are used to reconstruct each mode, respectively (Fig. 1; Table 1).

After performing a climate-growth correlation analysis, 27 out of 44 chronologies in Russia (Altai), 6 out of 12 in Kyrgyzstan, 9 out of 10 in western Mongolia and 6 out of 15 in westernmost China were retained for regression

analysis (Fig. 1). In total, 38 out of 81 chronologies (48 predictors out of 162) were used for the following analysis (Table 1). The first 11 eigenvectors with eigenvalues greater than 1 derived from the 48 predictors were retained in the final reconstruction model during the most replicated period from 1802 to 1992. The number of predictors (tree-ring chronologies of the previous and current years) varies from 48 for the most replicated period from 1802 to 1992 to 11 from 1587 to 1992 (Fig. 5). The reconstructed PDSI explains 54% of the total variance over the common period from 1951 to 1992 (Fig. 5). Accordingly, the full period calibration statistics (e.g. r square) generally weaken in significance back into time. Statistics for two split calibration–verification tests: 1950–1981 and 1982–1992, and 1963–1992 and 1951–1962 are shown in Fig. 5. The instrumental PDSI from 1993 to 2005 were appended to the reconstruction estimates for comparison with past drought variability. The final PDSI time series for the western mode spans from 1587 to 2005 (Fig. 5). Significant ($p < 0.05$) spectral peaks of this reconstruction were found at inter-annual (~ 2 –3 and 4–8 years) and decadal scales (11.4 and 16.5 years). Correlation between our west mode reconstruction and the previous published far-western Mongolia drought reconstruction is 0.42 ($p < 0.01$) during their common period of 1587–2003 (Fig. 7).

With regards to the eastern mode drought reconstruction, 19 of 49 candidate chronologies were retained (Table 1). That is, 14 out of 20 chronologies and 19 out of 40 predictors in Mongolia, as well as 5 out of 29 chronologies and 6 out of 58 predictors in China, entered into the reconstruction model (Fig. 1). Seven eigenvectors with eigenvalues greater than 1 were selected to reconstruct the leading drought mode during the most replicated period. As shown in Fig. 6, the number of predictors decreases from 25 over 1795–1989 to 20 for 1660–1989. The reconstruction explains 44% of the instrumental variance for the common period of 1951–1989 (Fig. 6). Calibration–verification statistics for two split eastern mode reconstructions show time-varying model reliability: 1950–1981 and 1982–1992, and 1963–1992 and 1951–1962 are shown in Fig. 6.

Table 2 Variances explained by the eigenvectors before and after the varimax rotation

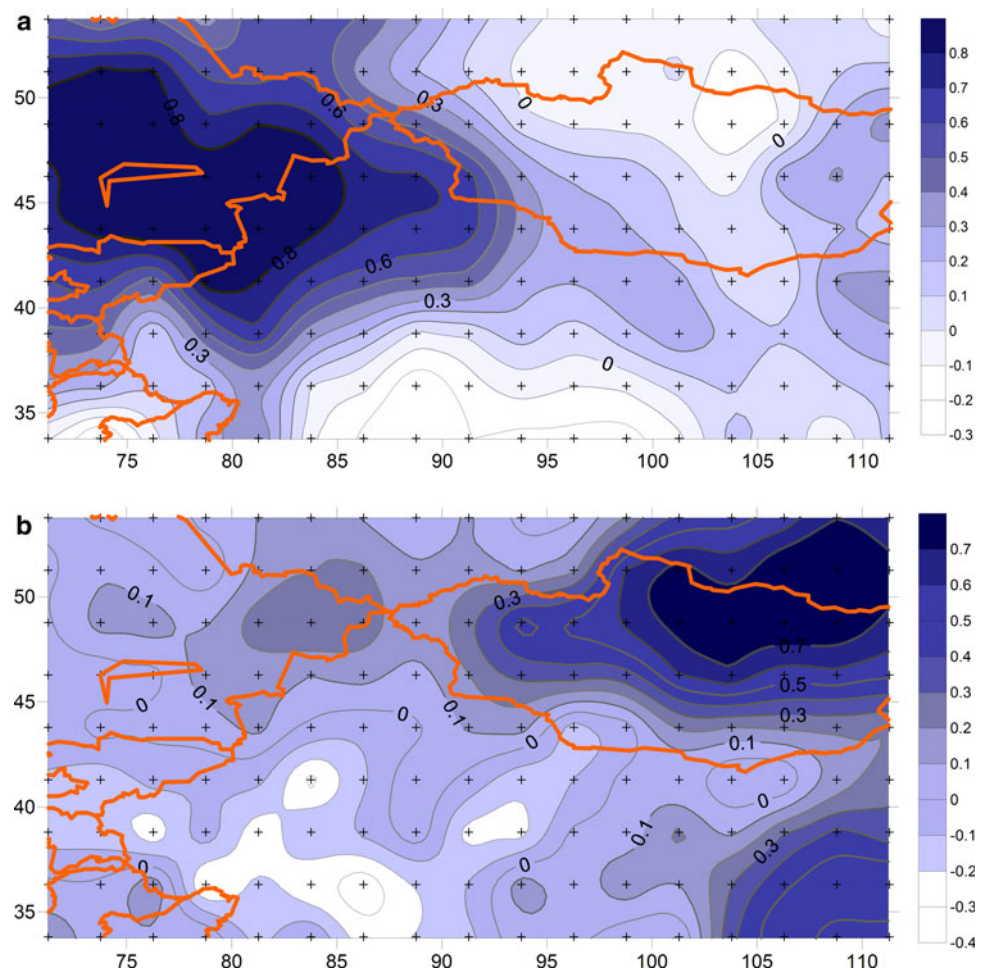
Initial values				Rotation sums of squared loadings		
Component	Eigenvalue	% of Variance	Cumulative %	Eigenvalue	% of variance	Cumulative %
1 ^a	35.9	23.5	23.5	28.7	18.8	18.8
2 ^a	18.9	12.3	35.8	15.3	10.1	28.8
1 ^b	29.3	32.5				
1 ^c	21.3	33.7				

^a The components from the PCA and RPCA for the entire central High Asia as identified in Fig. 2

^b The first principal component for the western central High Asia as identified in Fig. 3a

^c The first principal component for the eastern central High Asia as identified in Fig. 3b

Fig. 3 Maps showing RPCA factor loadings 1 (a) and 2 (b) for the central High Asia. The PDSI grids used in calculation were also shown



The final reconstruction for the eastern mode spans from 1660 to 2005 with the actual PDSI data from 1990 to 2005 appended for comparison. Significant ($p < 0.05$) cyclic patterns of the eastern mode reconstruction were identified from inter-annual (~ 3 – 5 , 6.2 and 8.2 years) to inter-decadal (34.1 years) and centennial (114 years) scales. Our eastern mode reconstruction showed high positive correlation ($r = 0.59$, $p < 0.01$) with the previous published Selenge streamflow reconstruction in Mongolia over the common period: 1660–1997 (Fig. 7). Running correlations between the reconstructed and 11-year smoothed west and east mode reconstructions are shown in Fig. 8.

4 Discussion

4.1 Calibration and verification testing

It is readily understood that the increase in MSL could lead to decline in averaged ring-width (Fig. 2a), because more old trees with narrow rings were included in calculation of AGR (Büntgen et al. 2008). It appears that *Juniperus* trees

generally show the longest MSL and lowest AGR. While the lowest MSL and highest AGR are found for *Picea* and *Pinus* trees (Fig. 2a). *Juniperus* trees distribute at significantly higher elevations than the other two categories (Fig. 2b). A decline in drought response at higher elevations may be because that the elevated precipitation for these sites alleviates the drought limitation on tree-growth (Fritts 1976). A weakness in climate responses for tree-growth at high-elevation sites was also documented by previous study in NW China (Gou et al. 2005).

The western and eastern drought patterns, as shown in Figs. 3 and 4, generally agree with previous west-east drought classifications for similar areas (Li et al. 2009; Qian and Qin 2008; Shi et al. 2007; Zou et al. 2005). The varying drought regimes within central High Asia indicate that it is more meaningful to reconstruct each drought mode separately. As indicated by high loadings and explained variance, the first PC is considered to represent the leading drought pattern of each mode. Therefore, we reconstruct the first PC of each mode using principal component regression (Fig. 4; Table 2). Both the western and eastern modes yield their lowest loadings over the

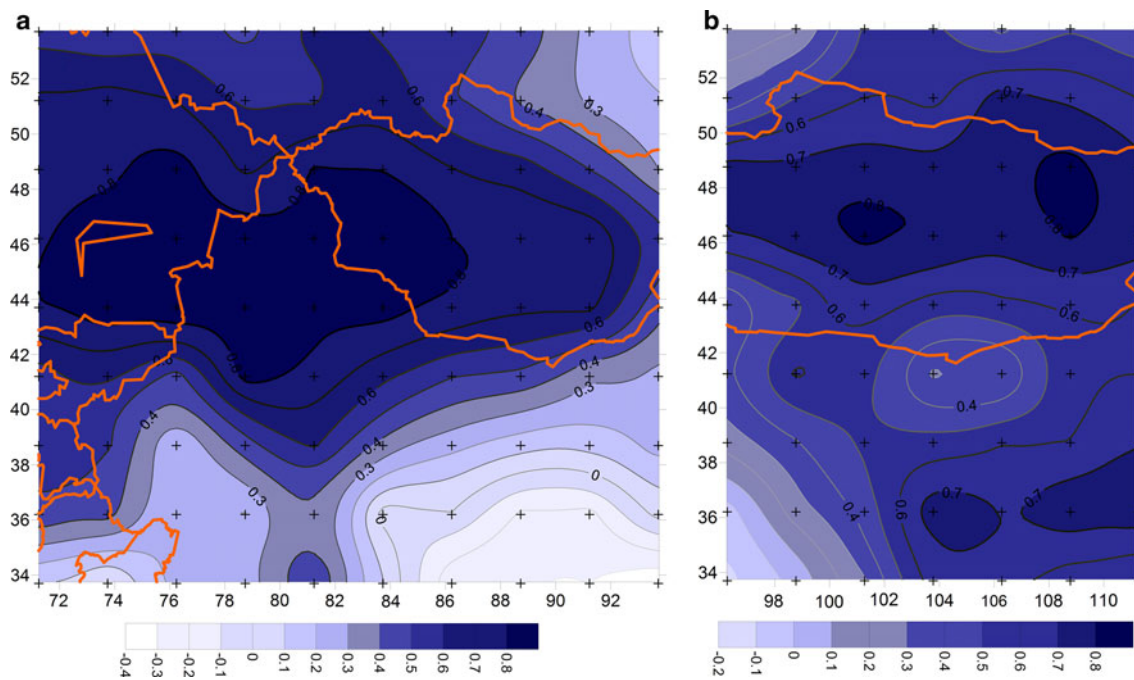
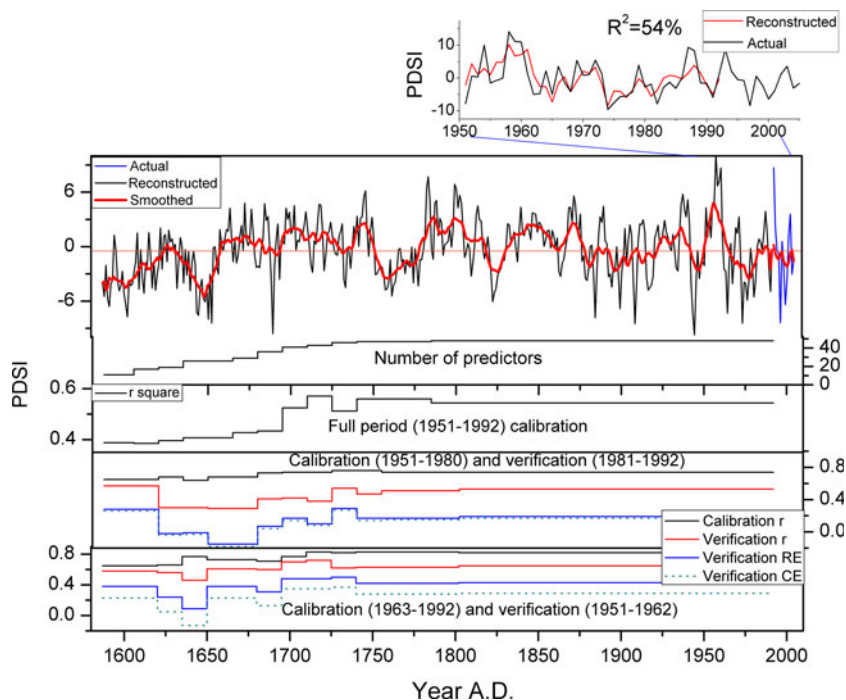


Fig. 4 Maps of first principal component loadings for the western (a) and eastern (b) central High Asia, as classified by RPCA in Fig. 3. The PDSI grids used in calculation were also shown

Fig. 5 PDSI reconstruction for the western central High Asia as classified by Fig. 4 over the time period of 1587–1992. Top two panels show the comparison between actual and reconstructed PDSI data, and the reconstructed and 11-year smoothed data via adjacent-averaging method. The actual PDSI from 1993 to 2005 are also shown. Bottom three panels show the time varying full period calibration and split calibration and verification results



northern Tibetan Plateau that is in the south of our study area (Fig. 3), indicating different moisture conditions on the plateau.

Many chronologies from Russia (Altai) and Mongolia were retained in the drought reconstruction model, suggesting a closer relationship between the leading drought modes and tree rings over these regions. This may

suggest that more drought sensitive tree rings were located in those dry areas. High PC loading over these regions might also have impacts on the drought-growth spatial patterns. The tree-ring chronologies that are not drought sensitive or not closely related to the leading drought patterns were excluded during this screening procedure. The PCA decomposition on the retained tree-

Fig. 6 Spatial PDSI reconstruction for the eastern central High Asia as shown in Fig. 4 over the period 1660–1989. *Upper two panels* present the comparison between actual and reconstructed PDSI data, and the reconstructed and 11-year smoothed data. The actual PDSI from 1990 to 2005 are also shown for comparison with variability during previous periods. *Lower three panels* show results of the time varying full period calibration and split calibration and verification. Note that the verification statistics for the period of 1981–1989 are calculated based on the first differenced data

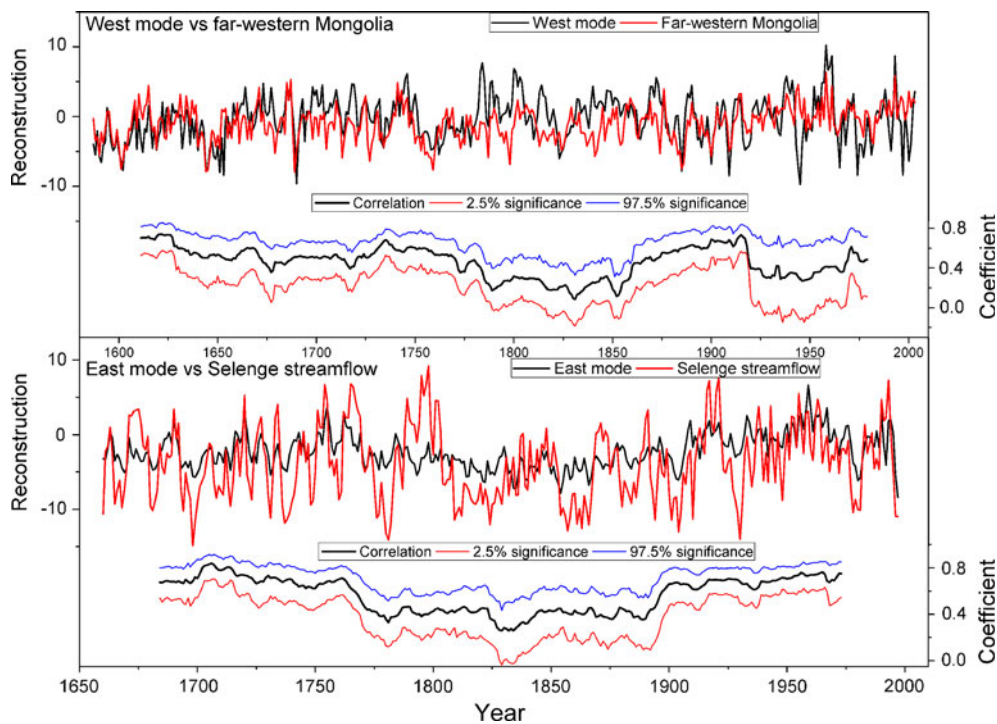
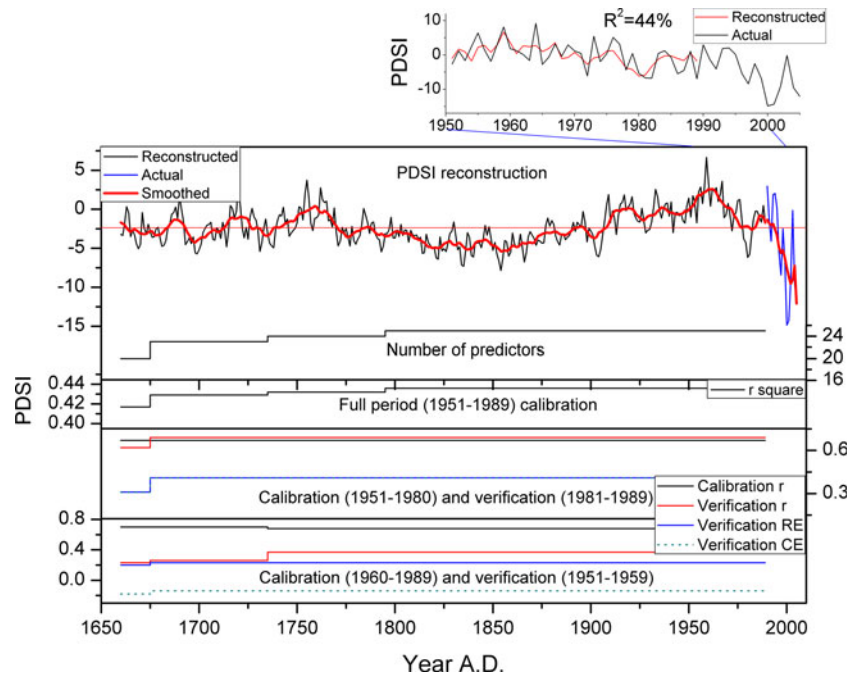


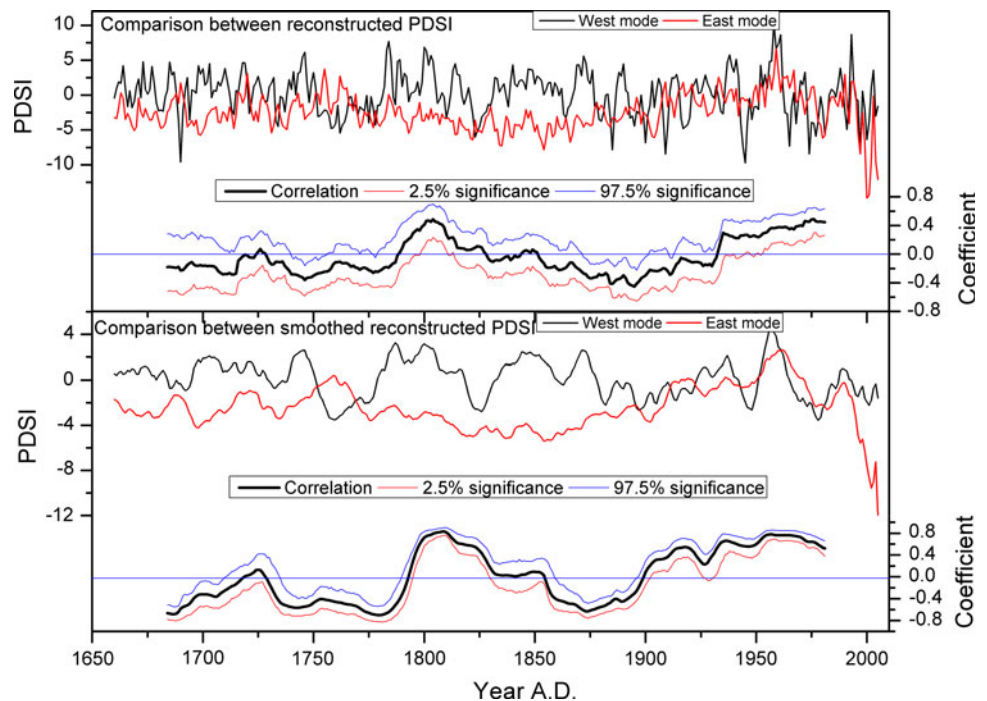
Fig. 7 Comparisons of our west and east mode reconstructions with far-western Mongolia drought reconstruction (*upper panel*) (Davi et al. 2009) and Selenge streamflow reconstruction (*lower panel*) (Davi et al. 2006), respectively. Note that the Selenge streamflow was

rescaled to meet the range of the drought reconstruction. Their associated running correlations based on a 51-year window are also listed

ring chronologies has resulted in reduced number of predictors (eigenvectors), which could again reduce the artificial predictability that results from the inclusion of too many predictors.

Calibration and verification test for most of the nested models are robust and relatively stable, indicating good model fits over time, but verification CE values are negative over some earlier periods, such as verification (1951–1962)

Fig. 8 Comparisons of reconstructed (*upper panel*) and 11-year smoothed reconstructed PDSI data (*lower panel*) between the western and eastern reconstructed drought modes over the common period 1660–2005, as derived from Figs. 4 and 5. Running correlations using a 51-year window for each comparison and the two-tailed 95% confidence intervals are also shown



results for 1635–1650 and verification (1981–1992) results for 1650–1675. However, relatively poor verification statistics for one sub-period often correspond to better verification results in the remaining time period. This means that such relatively poor nested model statistics are due to the varying model accuracy through the two split sub-periods. Nevertheless, statistics for the full calibration period are reasonably valid (Fig. 5). Therefore, we retained these nests in the final reconstruction based on the full period of calibration. Compared to the western mode reconstruction, the PDSI reconstruction for the eastern mode is less robust, as indicated by fewer retained predictors and a lower full period r square (Fig. 6). However, the number of predictors and the resultant statistics for different nests are more stable than for the western mode reconstruction (Fig. 6). Due to early nests with relatively poor but less variable model fits, we truncated the eastern mode reconstructions at 1660, when the full period r square still exceeds 41.7%. It should be noted that values of the rigorous CE statistic for the nests are negative for the calibration (1960–1989) and verification (1951–1959). We attribute this to the abnormal drying trend in recent decades. That is, according to the definition of the CE statistics, the big differences in mean values between the two split sub-periods lead to extraordinarily low values of the denominators of the calculation for CE. This could, in turn, result in the abnormally low values of CE. This phenomenon has been documented by previous PDSI reconstructions for similar areas (e.g. Fang et al. 2009a). However, this situation could be alleviated by using the full period calibration with data from two split sub-periods.

4.2 Drought variability

The most severe dry epoch for the western mode reconstruction occurs during the 1640s to 1650s (Fig. 5). This mega-drought precedes the start of the eastern mode reconstruction in 1660 (Fig. 6). However, a cave record for central China, close to the identified eastern mode, suggests that this dry epoch may also have been the most extreme for the eastern mode over the past 400 years (Zhang et al. 2008). This result indicates that the prominent 1640s to 1650s dry epoch may have covered much of central High Asia. The collapse of the Chinese Ming Dynasty in 1644 occurred during this drought epoch, suggesting possible links between droughts and cultural changes. Such severely dry conditions may have largely reduced the commissariat supply and thus led to the peasant unrest against the Chinese Ming Dynasty at that time (Zhang et al. 2008). However, we also stress caution, because our reconstruction can only reveal moisture conditions for the westernmost area of the Chinese Ming Dynasty. The wettest epochs for both the western and eastern reconstructions are found in the 1950s (Figs. 5, 6), indicating a large area influenced by extreme wet conditions. With regards to the western mode reconstruction, other severe dry intervals (with 11-year smoothed data lower than $-2SD$ at -3.6) occurred in the 1590s to 1600s, 1760s, 1970s, and other abnormally wet conditions (greater than $2SD$ at 2.9) in the 1780s to 1790s.

The eastern mode reconstruction shows more centennial variations (Fig. 6). In general, the reconstructed PDSI

fluctuate around the mean prior to the eighteenth century; and the PDSI values fall below normal for the nineteenth century. Wet conditions are observed for the early half of the twentieth century, while a dramatic drying trend is seen in the three most recent decades (Fig. 6). The western and eastern mode reconstructions are more variable in recent decades, consistent with previous studies in these areas (e.g. Fang et al. 2009a; Li et al. 2007). Both the driest and wettest epochs over the length of reconstruction occurred in recent decades, e.g. wet epoch for the 1950s–1960s and a dry epoch after the 1980s for eastern mode (Fig. 6). This may suggest that moisture conditions of central High Asia have become more variable in response to recent climate warming. The wetting and drying trends are also seen for the western mode reconstruction, but the drying trend since the 1980s is evident. This is because an increase in precipitation over the western mode (Shi et al. 2007) and vicinity (Treydte et al. 2006) has alleviated the drought caused by increase in temperature. The distinct drying trend since the 1980s has been documented by many studies, especially in the eastern region (Fang et al. 2009a, b; Li et al. 2007; Shi et al. 2007; Zhang et al. 2008; Zou et al. 2005). Our study further suggests that this drying trend is the most severe event that has occurred over the past 346 years for the whole eastern region. Possible factors accounting for this drying trend include the weakening of the Asian monsoon (Kripalani et al. 2003; Zhang et al. 2008), anthropogenic forcing (Zhang et al. 2008), and/or effects of intensified evaporation induced by recent global warming. Since regional droughts are mainly controlled by the Asian monsoon systems (e.g. Fang et al. 2009b; Shi et al. 2007; Zhang et al. 2008), the weakening of the Asian monsoon may be the main cause for recent severe drying trend in the eastern mode.

More significant low-frequency spectral peaks were found for the eastern mode reconstruction, consistent with the above analysis that this reconstruction retains more low-frequency information. However, statistically significant spectral peaks at the centennial time scale for the eastern mode reconstruction may not be realistic because the overall length of the series is only 336 years. Spectral peaks of 34.1-year that are close to the inter-decadal spectral feature of the Pacific Decadal Oscillation (PDO) and the inter-decadal mode of the North Pacific sea surface temperatures (D'Arrigo and Wilson 2006; Li et al. 2004) suggest possible teleconnections with remote ocean conditions. Actually, many tree-ring chronologies used for the eastern mode reconstruction were also employed for a PDO reconstruction based on Asian tree-ring data (D'Arrigo and Wilson 2006). Significant decadal spectral peaks at ~ 11.5 years for the western mode reconstruction are close to the sunspot cycle (Fig. 8a), indicating possible links of regional droughts to solar activity. Significant inter-annual

spectral peaks of 3–8 years for both the western and eastern mode reconstructions fall within the broader bandwidth of 2–11 years for ENSO (Allan 2000). Previous studies revealed mechanisms that may explain the influence of ENSO on rainfall in north China (Li and Zeng 2002; Lu 2005). However, linkages between the western mode reconstruction and ENSO are uncertain.

4.3 Drought comparisons

As shown in Fig. 7, both of our spatial reconstructions show similar variability to the previous reconstructions (Davi et al. 2006, 2009) for geographic points within each mode (Fig. 7). It should be noted that the Selenge streamflow variations are rescaled to have the same range as the PDSI variability. The similar pattern between this study and the Selenge streamflow reconstruction is reasonable, because the first PC of each mode shows high loadings over these regions (PDSI gridpoint at 48.75 N 88.75E and streamflow station at 49.34 N 101.31E) as shown in Fig. 4. However, relatively low correlations between our reconstructions and point reconstructions are found at some periods, such as the ~ 1820 s for both comparisons (Fig. 7). This may suggest that the two previous reconstructions for geographic points account for relatively little variance of the spatial common patterns during these periods.

Although significant positive correlations between point reconstructions and field reconstructions suggest homogeneity within each mode, there is heterogeneity between the two drought modes according to the non-significant correlations between the reconstructions from both western and eastern modes. Actually, reconstructions of much longer time scales that were based on other climate archives, e.g. pollen and lake levels, also documented the distinct difference between the two drought modes (Chen et al. 2008). Those studies also suggested different forcings between the two drought modes, consistent with the above RPCA results. However, there are relatively high positive running correlations during certain periods, for example, at the 1790s to 1800s and after the 1940s. These two intervals coincide with the two wettest periods in the western reconstruction, with the wettest conditions for the 1940s to 1950s (Figs. 5, 6). It seems that the positive correlations tend to occur at periods when the western mode reconstruction is under wet conditions. Both series show a drying trend since the 1980s, albeit there is a much stronger decline trend for the eastern mode reconstruction (Fig. 8). Negative values are seen during the 1740s to 1750s, 1770s and 1870s to 1900s (Fig. 8). These negative correlations appear to occur at periods when the western mode is relatively dry (Fig. 5). Running correlations for reconstructed and smoothed reconstructed data show roughly similar

patterns but with some disagreements, e.g. before the 1700s (Fig. 8).

5 Conclusions

We classified the drought patterns of a PDSI network with 153 grids for central High Asia (70E–112E, 33N–52N), using RPCA. The identified western and eastern drought modes are delimited at $\sim 93.75\text{E}$. The first principal component of each mode was reconstructed, using tree-ring chronologies located within each mode. 38 out of 81 candidate chronologies were employed to reconstruct the western drought mode, extending back to 1587. The western reconstruction explains 54% of the instrumental PDSI variance, and statistics of calibration and verification tests are found to be reasonably valid for the nested datasets. 19 of 49 candidate chronologies were utilized to extend the eastern mode back to 1660, i.e. from 1660 to 2005. The reconstructed PDSI accounts for 44% of instrumental PDSI variance for the eastern mode reconstruction. Compared to the western mode reconstruction, the time-varying statistics are somewhat less rigorous but more stable due to the relatively smaller but constant number of chronologies entered into the reconstruction model.

Our spatial reconstructions show variability consistent with previous reconstructions at geographic points within these classified regions, while no significant correlation was found between the reconstructions of the classified western and eastern modes. Both spatial reconstructions show greater variability in recent decades. The wettest periods for both reconstructions are found from the 1940s to 1950s. Running correlations over the common period from 1660 to 2005 are relatively higher when the western mode was in wet conditions. The driest epoch for the western mode reconstruction occurred from the 1640s to 1650s, coinciding with the time of the collapse of the Chinese Ming Dynasty. The driest epoch for the eastern mode reconstruction occurs since the 1980s. Both reconstructions have shown significant cycles at interannual to interdecadal scales, as identified by spectral analyses. Interdecadal variability at ~ 34.1 years in the eastern mode reconstruction may suggest the influence of the PDO for this region. Interannual scale spectral peaks from 3 to 8 years for the eastern mode reconstruction fall within the broad bandwidth of the ENSO variability.

Acknowledgments The authors acknowledge Fritz Schweingruber, Gordon Jacoby, Jan Esper, Paul Sheppard, Xuemei Shao, Neil Pederson, and some other scientists who have contributed their tree-ring data for this study. We thank Ken Peters for his kind helps on language improvements. Constructive comments and suggestions from two anonymous reviewers are highly appreciated. This research was supported by the National Science Foundation of China

(No. 40971119), the US National Science Foundation (No. ATM0117442 & ATM-0402474), the NSFC Innovation Team Project (No. 40721061), the Chinese 111 Project (B06026), and the One Hundred Talents Program of CAS (Grant No. 290827B11).

References

- Allan R (2000) ENSO and climatic variability in the past 150 years. In: Diaz H, Markgraf V (eds) *El Niño and the Southern Oscillation: Multiscale Variability and Global and Regional Impacts*. Cambridge University Press, Cambridge, pp 3–56
- Briffa KR, Jones PD, Wigley TML, Pilcher JR, Baillie MGL (1986) Climate reconstruction from tree rings. Part 2. Spatial reconstruction of summer mean sea-level pressure patterns over Great Britain. *J Climatol* 6:1–15
- Büntgen U, Frank D, Wilson R, Carrer M, Urbinati C, Esper J (2008) Testing for tree-ring divergence in the European Alps. *Global Change Biol* 14:2443–2453
- Chen F, Yu Z, Me Yang, Ito E, Wang S, Madsen DB, Huang X, Zhao Y, Sato T, Birks J, Boomer I, Chen J, An C, Wünnemann B (2008) Holocene moisture evolution in arid central Asia and its out-of-phase relationship with Asian monsoon history. *Quaternary Sci Rev* 27:351–364
- Cook ER (1985) A time-series analysis approach to tree-ring standardization. PhD dissertation, The University of Arizona, Tucson
- Cook ER, Briffa KR, Jones PD (1994) Spatial regression methods in dendroclimatology: a review and comparison of two techniques. *Int J Climatol* 14:379–402
- Cook ER, Meko DM, Stahle DW, Cleaveland MK (1999) Drought reconstructions for the continental United States. *J Clim* 12:1145–1162
- Cook ER, D'Arrigo RD, Mann ME (2002) A well verified, multiproxy reconstruction of the winter North Atlantic Oscillation Index since AD 1400. *J Clim* 15:1754–1764
- Cook ER, Woodhouse CA, Eakin CM, Meko DM, Stahle DW (2004) Long-term aridity changes in the western United States. *Science* 306:1015–1018
- D'Arrigo R, Wilson R (2006) On the Asian expression of the PDO. *Int J Climatol* 26:1607–1617
- D'Arrigo R, Jacoby GC, Pederson N, Frank D, Buckley B, Nachin B, Mijiddorj R, Dugarjav C (2000) Mongolian tree rings, temperature sensitivity and reconstructions of Northern Hemisphere Temperature. *Holocene* 10(6):669–672
- Dai AG, Trenberth KE, Qian T (2004) A global dataset of Palmer Drought Severity Index for 1870–2002: relationship with soil moisture and effects of surface warming. *J Hydrometeorol* 5:1117–1130
- Davi NK, Jacoby GC, Curtis AE, Baatarbileg N (2006) Extension of drought records for Central Asia using tree-rings: West Central Mongolia. *J Clim* 19:288–299
- Davi NK, Jacoby GC, D'Arrigo R, Baatarbileg N, Li J, Curtis AE (2009) A tree-ring-based drought index reconstruction for far-western Mongolia: 1565–2004. *Int J Clim* 29:1508–1514
- Davi NK, Jacoby GC, D'Arrigo R, Li J, Robinson, Fang K (2010) Reconstructed drought across Mongolia based on large-scale network of tree-ring records: 1693–1993 (in review)
- Fang K, Gou X, Chen F, Yang M, Li J, He M, Zhang Y, Tian Q, Peng J (2009a) Drought variations in the eastern part of Northwest China over the past two centuries: evidence from tree rings. *Clim Res* 38:129–135
- Fang K, Gou X, Chen F, D'Arrigo R, Li J (2009b) Tree-ring based drought reconstruction for Guiqing Mountain (China): linkage to

- the Indian and Pacific Oceans. *Int J Climatol*. doi: [10.1002/joc.1974](https://doi.org/10.1002/joc.1974)
- Fritts HC (1976) *Tree Rings and Climate*. Academic Press, London
- Fritts HC (1991) *Reconstructing large-scale climate patterns from tree-ring data*. The University of Arizona Press, Tucson, p 286
- Gou X, Chen F, Yang M, Li J (2005) Climatic response of tree-ring width at different elevations over Qilian Mountains, northwestern China. *J Arid Environ* 61:513–524
- Haston L, Michaelsen J (1997) Spatial and temporal variability of southern California precipitation over the last 400 yr and relationships to atmospheric circulation patterns. *J Clim* 10:1836–1852
- Kripalani RH, Ashwini K, Sabade SS (2003) Indian monsoon variability in a global warming scenario. *Nat Hazards* 29:189–206
- Li JP, Zeng Q (2002) A unified monsoon index. *Geophys Res Lett* 29(8):1274. doi: [10.1029/2001GL013874](https://doi.org/10.1029/2001GL013874)
- Li C, He J, Zhu J (2004) A review of decadal/interdecadal climate variation studies in China. *Adv Atmos Sci* 21(3):425–436
- Li J, Gou X, Cook ER, Chen F (2006) Tree-ring based drought reconstruction for the Central Tien Shan Area, Northwest China. *Geophys Res Lett* 33:L07715. doi: [10.1029/GL025803](https://doi.org/10.1029/GL025803)
- Li J, Chen F, Cook ER, Gou X, Zhang Y (2007) Drought reconstruction for north central China from tree rings: the value of the Palmer drought severity index. *Int J Climatol* 27:903–909
- Li J, Cook ER, D'Arrigo R, Chen F, Gou X (2009) Moisture variability over China and Mongolia: 1951–2005. *Clim Dyn*. doi: [10.1007/s00382-008-0436-0](https://doi.org/10.1007/s00382-008-0436-0)
- Liu Y, Ma L, Leavitt SW, Cai Q, Liu W (2004) A preliminary seasonal precipitation reconstruction from tree-ring stable carbon isotopes at Mt. Helan, China, since AD 1804. *Global Planet Change* 41:229–239
- Lu R (2005) Interannual variation of north China rainfall in rainy season and SSTs in equatorial eastern Pacific. *Chin Sci Bull* 50(18):2069–2073
- Mann ME, Lee JM (1996) Robust estimation of background noise and signal detection in climatic time series. *Clim Change* 33:409–445
- Meko DM, Graybill DA (1995) Tree-ring reconstruction of Upper Gila River discharge. *Water Resour Bull* 31(4):605–616
- Meko DM, Cook ER, Stahle DW, Stockton CW, Hughes MK (1993) Spatial patterns of tree-growth anomalies in the United States and southeastern Canada. *J Clim* 6:1773–1786
- Palmer WC (1965) *Meteorological drought*. Weather bureau research paper 45. US Department of Commerce, Washington, DC
- Qian WH, Qin A (2008) Precipitation division and climate shift in China from 1960 to 2000. *Theor Appl Climatol* 93:1–17
- Richman MB (1986) Rotation of principal components. *J Clim* 6:293–335
- Shi Y, Shen Y, Kang E, Li D, Ding Y, Zhang G, Hu R (2007) Recent and future climate change in northwest China. *Clim Change* 80:379–393
- Tian Q, Gou X, Zhang Y, Peng J, Chen T, Wang J (2007) Tree-ring based drought reconstruction for the Qilian Mountains, northwestern China. *Tree-ring Res* 63(1):27–36
- Treydte KS, Schleser GH, Helle G, Frank DC, Winiger M, Haug GH, Esper J (2006) The twentieth century was the wettest period in northern Pakistan over the past millennium. *Nature* 440:1179–1182
- Yuan YJ, Jin LY, Shao XM, He Q, Li ZZ, Li JF (2003) Variations of the spring precipitation day numbers reconstructed from tree rings in the Urumqi River drainage, Tianshan Mts. over the last 370 years. *Chin Sci Bull* 48(14):1507–1510
- Zhang P, Cheng H, Edwards L et al (2008) A test of climate, sun and culture relationships from an 1810-yr Chinese cave record. *Science* 322:940–942
- Zou X, Zhai P, Zhang Q (2005) Variations in droughts over China: 1951–2003. *Geophys Res Lett* 32:L04707. doi: [10.1029/2004GL021853](https://doi.org/10.1029/2004GL021853)